*Sensors and Materials*, Vol. 35, No. 2 (2023) 377–389
MYU Tokyo



S & M 3174

# Development and Simulation of Operational Scenarios for Underwater Cable-driven Parallel Robot

Katutoshi Kodama,* Akihiro Morinaga, and Ikuo Yamamoto

Graduate School of Engineering, Nagasaki University, 1-14 Bunkyo, Nagasaki 852-8521, Japan

(Received December 12, 2022; accepted February 1, 2023)

***Keywords:*** cable-driven, parallel robot, underwater robot, operation scenario, feedback control

A cable-driven parallel robot (CDPR) is a mechanism that controls the position and attitude of an object using multiple cables. We propose an underwater cable-driven parallel robot (UCDPR), which is a CDPR composed of multiple surface robots. A UCDPR is a type of mobile cable-driven parallel robot (MCDPR) that is composed of multiple mobile robots and is an underwater application of MCDPR, which has been used only on land and in the air. We describe the details of the operational scenario of the UCDPR, from landing on the water to executing a task. We also simulated numerically the stabilization phase required after landing on water and the trajectory tracking control phase required for underwater exploration and other tasks. In this numerical simulation, we used a high-gain feedback controller as the trajectory tracking controller to add robustness to the control system. As a result, a trajectory tracking control was realized within a tolerance tracking error range of $10^{-2}$ m underwater in the presence of a maximum current velocity of 0.8 m/s (≅ 1.5 knots), which is a control requirement.

## 1. Introduction

A cable-driven parallel robot (CDPR) is a type of parallel mechanism that uses multiple cables to constrain an object and control its position and attitude by controlling the cable lengths.[1,2] When lightweight and flexible cables are used, the mechanism is lightweight and can achieve a large payload capacity and function in a large workspace.

A CDPR consisting of multiple mobile robots is called a mobile cable-driven parallel robot (MCDPR).[3] An MCDPR is different from a typical CDPR in that it has kinematic redundancy in its mechanism because the cable feed position can be actively changed by the controller. By appropriately using kinematic redundancy, an MCDPR can do sub-tasks such as obstacle avoidance and singularity avoidance in addition to the main task of trajectory tracking control. The MCDPR has been applied to FASTKIT[4] and MoPICK (Mobile Pick-and-Place),[5] which do pick-and-place operations in factories, and to mechanisms that coordinate multiple aerial robots to do transportation and rescue operations.[6,7] As described above, MCDPR has been considered for many applications on land and in the air, but not much thought has been given to its application underwater. One of the reasons for this is that the drag force and water currents on

*Corresponding author: e-mail: bb52221102@ms.nagasaki-u.ac.jp
https://doi.org/10.18494/SAM4280

ISSN 0914-4935 
https://myukk.org/

the object underwater are large and deform the cable, making it difficult to control the position of the suspended object.

To solve the problem of underwater application of MCDPR, we proposed an underwater cable-driven parallel robot (UCDPR), which is composed of multiple robots that work on the surface of the water [autonomous surface vehicles (ASVs), unmanned surface vehicles (USVs), and others],[8] and developed a modeling method for the mechanism that takes into account cable dynamics underwater[9,10] and for a basic control system configuration.[10,11]

To operate the UCDPR in an actual environment, it is necessary to consider operational scenarios[12,13] from the landing of the robot on the water to the execution of the objective task (or the recovery of the robot), just as one must consider with general underwater robots [such as remotely operated vehicles (ROVs) and autonomous underwater vehicle (AUVs)], and to design an appropriate controller for each scenario. Therefore, we have developed a scenario based on the operation of a UCDPR in an actual environment and have performed control simulations based on this operational scenario. To simplify the discussion, we assumed that the vertical movement of the water surface due to waves on the water may be disregarded.

## 2. Overview of a UCDPR

### 2.1 Mechanism

Figure 1 shows a conceptual diagram of our proposed UCDPR. This UCDPR is an underwater application of an MCDPR using multiple surface robots. A UCDPR with the configuration shown in Fig. 1 can control the position and attitude (six degrees of freedom) of a suspended object in three-dimensional space.

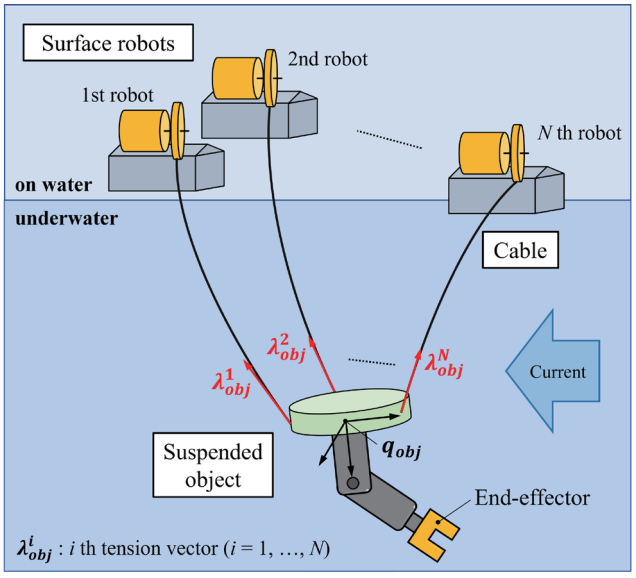


Fig. 1. (Color online) Image of a UCDPR.

In our UCDPR, the surface robot's position is measured by the Global Positioning System (GPS), and the cable lengths are measured by a rotary encoder. For a typical CDPR, the position and attitude of the suspended object can be easily estimated from the geometric relationships to the CDPR. However, underwater, it is difficult to accurately estimate the position and attitude of a suspended object because of the effect of currents. Therefore, the position of the suspended object was measured by acoustic positioning, and its attitude was measured by a gyro sensor.

## 2.2 Experimental device

Figure 2 shows the exterior and system configuration of the experimental device. Figure 2(a) shows the experimental device, which is composed of two trolleys at the top of the frame. Two cables are played out from each trolley to control the position of the suspended object on a two-dimensional surface. The two trolleys are attached to independent timing belts, which move left and right along the guide rails. These timing belts are actuated by DC motors. Winches are attached to the top of the trolleys to control the cable lengths. These winches are actuated by DC servo motors. All motors have hall encoders to measure the displacement of the trolley and the reeling length of the cables from the angle of rotation of the motors.

The position of the suspended object is measured by acoustic positioning in actual environments. However, the experimental device shown in Fig. 2(a) is too small to have an acoustic positioning system installed. Therefore, image processing (color tracking) using augmented reality (AR) markers attached to the four corners of the experimental device and color tape attached to the suspended object is used to obtain the position of the suspended object in real time.

The experimental device is also attached to a commercially available water pump to simulate water currents. Although analysis of the velocity distribution is currently underway, the experimental device enables control experiments that simulate actual conditions at sea.

Figure 2(b) shows a diagram of the control system of this experimental device. The control system is composed of a Python-based control system on a computer (host system) and a control system on a control board (Arduino Mega) attached to the experimental device (low-order system). The host system and the low-order system exchange control command values and

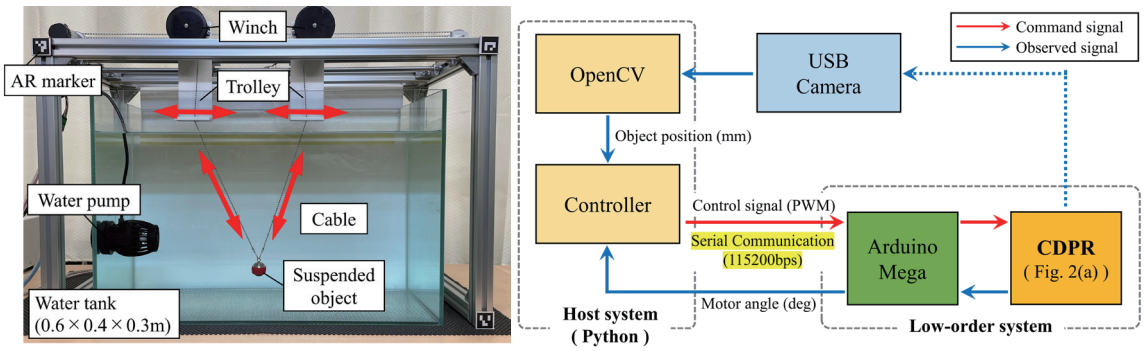


(a) (b)

Fig. 2. (Color online) (a) Experimental device and (b) system configuration of the experimental device.

sensor values via serial communication. The host system (computer) acquires the position of the suspended object by image processing of the video captured by the USB camera. Using the position of the suspended object, the cable lengths, and the position of the trolley sent from the experimental device, the computer calculates the manipulated variable and sends the pulse width modulation (PWM) value to the low-order system (Arduino Mega). The low-order system controls the actuator according to this PWM value and sends the rotation angle of the motor to the host system (computer). The control period of the experimental device is determined by the frames per second (FPS) of the USB camera and the time required for image processing. The control period of the control system used was 0.1 s.

## 3. Development of Operational Scenarios

The operational scenario assumed the basic operation of the UCDPR in an actual environment (especially in the sea). A UCDPR realizes a chain of motion control from UCDPR landing on the water to task execution by switching controllers according to each scenario. Although Fig. 3 shows only the motion of the UCDPR on a two-dimensional surface for the simplification of the explanation, the same argument can be made in the actual environment (three-dimensional space).

### 3.1 Scenario A: Calibration of mechanism and positioning control

Because the UCDPR is a mechanism composed of multiple surface robots and a suspended object, it was difficult to accurately pinpoint the landing site on water of all components when landing the UCDPR from the ground or a mother ship, even if the landing position was planned in advance. In addition, there was a concern that the suspended object may sway underwater because of the currents. Therefore, in Scenario A, calibration of the initial positions of the surface robots and other components and positioning control of the suspended object underwater was carried out to stabilize the mechanism. At the same time, we also checked the sensors and communication system.

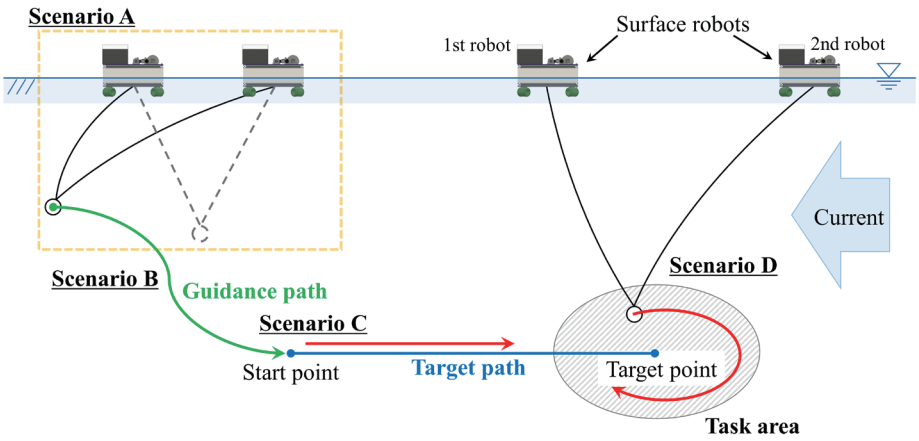


Fig. 3. (Color online) Diagram of operational scenario.

### 3.2 Scenario B: Guidance and control

In Scenario B, the UCDPR was guided from its initial position, which was held in place by Scenario A, to the target position (e.g., the start of the reference path in Scenario C or the target position in the work area in Scenario D). Guidance control of the UCDPR was achieved by calculating the guidance path (trajectory) that smoothly connected the initial position and the target position in real time and controlling UCDPR autonomously to track this guidance path.

### 3.3 Scenario C: Trajectory tracking control

In Scenario C, the trajectory tracking control of the UCDPR was carried out according to a preplanned path (trajectory). The UCDPR trajectory tracking control system must be robust against parameter errors, modeling errors, and variations in current velocity.

### 3.4 Scenario D: Execution of objective tasks

In Scenario D, the UCDPR carried out an arbitrary task at a preplanned target point by positioning the surface robots and controlling the cable lengths. The objective task was done by remote control from the ground or mother ship, or by autonomous control of the UCDPR. Concrete tasks were expected to include underwater fixed-point observation and installation of underwater structures.

## 4. Numerical Simulation Based on Operational Scenarios

We numerically simulated a simple operational example composed of Scenario A and Scenario C for the experimental device shown in Fig. 2(a).

### 4.1 Mathematical models

First, the dynamics model of the entire UCDPR to be used as the control object of the numerical simulation is given by Eq. (1). For a detailed derivation of this equation, refer to Ref. 10.

$$\begin{bmatrix} \boldsymbol{M}(\boldsymbol{q}) & -\boldsymbol{G}^{T}(\boldsymbol{q}) \\ \boldsymbol{G}(\boldsymbol{q}) & \boldsymbol{0} \end{bmatrix} \begin{bmatrix} \ddot{\boldsymbol{q}} \\ \boldsymbol{\lambda} \end{bmatrix} = \begin{bmatrix} \boldsymbol{F} \\ \boldsymbol{\gamma} \end{bmatrix} \tag{1}$$

Here, $\boldsymbol{q}$ is the state vector of the position and attitude of the entire UCDPR, $\boldsymbol{M}(\boldsymbol{q})$ is the mass matrix, and $\boldsymbol{F}(\boldsymbol{q})$ is a vector of generalized forces. The terms $\boldsymbol{G}(\boldsymbol{q})$ and $\boldsymbol{\gamma}$ are defined by the holonomic constraint $\boldsymbol{\Phi}(\boldsymbol{q}) = \boldsymbol{0}$ for the entire mechanism as

$$\dot{\boldsymbol{\Phi}}(\boldsymbol{q}) = \frac{\partial \Phi}{\partial \boldsymbol{q}} \dot{\boldsymbol{q}} = \boldsymbol{G}(\boldsymbol{q}) \dot{\boldsymbol{q}}, \tag{2}$$

$$\ddot{\boldsymbol{\Phi}}(\boldsymbol{q}) = \boldsymbol{G}(\boldsymbol{q}) \ddot{\boldsymbol{q}} + \dot{\boldsymbol{G}}(\boldsymbol{q}) \dot{\boldsymbol{q}}, \tag{3}$$

and

$$\boldsymbol{\gamma} = -\dot{\boldsymbol{G}}(\boldsymbol{q}) \dot{\boldsymbol{q}} - 2\alpha \boldsymbol{G}(\boldsymbol{q}) \dot{\boldsymbol{q}} - \beta^2 \boldsymbol{\Phi}(\boldsymbol{q}), \tag{4}$$

where $\boldsymbol{\Phi}(\boldsymbol{q}) = \boldsymbol{0}$ is a position constraint, Eq. (2) is a velocity constraint, and Eq. (3) is an acceleration constraint. Equation (4) is a Baumgarte stabilization term that reduces numerical errors and has $\alpha > 0$ and $\beta \geq 0$.

Next, we describe the inverse kinematics problem around a suspended object of UCDPR, which is necessary for the controller design. The inverse kinematics problem for UCDPR is different from that for CDPR because it requires solving the inverse dynamics problem in the calculation. Therefore, the inverse kinematics problem of UCDPR is an inverse kinematics problem in the broadest sense. For a detailed discussion of this problem, refer to Ref. 10. The solution of the inverse kinematics around the suspended object is given by

$$\dot{\boldsymbol{\kappa}} = \boldsymbol{J}_{obj}(\boldsymbol{q}_{obj}, \boldsymbol{\lambda}_{obj}) \dot{\boldsymbol{q}}_{obj} \triangleq \boldsymbol{J}_{obj}(\boldsymbol{q}_{obj}, \boldsymbol{\lambda}_{obj}) \boldsymbol{u} \tag{5}$$

and

$$\boldsymbol{\lambda}_{obj} = \boldsymbol{G}_{obj}^{+T} (\boldsymbol{M}_{obj} \ddot{\boldsymbol{q}}_{obj} - \boldsymbol{F}_{obj}) + \boldsymbol{h}_{obj} \boldsymbol{k}_{obj}, \tag{6}$$

where $\boldsymbol{q}_{obj}$ is the state vector of the position and attitude of the suspended object, and $\boldsymbol{\kappa}$ is a vector of the position of the trolleys and the cable lengths, which are manipulated variables of the UCDPR. The term $\boldsymbol{u}$ is a virtual control input in the kinematics controller, and by giving an appropriate feedback input, the manipulated variables $\boldsymbol{\kappa}$ can be calculated while reducing the effects of disturbances. The term $\boldsymbol{J}_{obj}$ is a matrix that expresses the velocity relationship between $\boldsymbol{q}_{obj}$ and $\boldsymbol{\kappa}$, and is represented by the manipulation force (tension) $\boldsymbol{\lambda}_{obj}$ on the suspended object, which is the inverse dynamics solution of Eq. (6). In Eq. (6), $\boldsymbol{M}_{obj}$ and $\boldsymbol{F}_{obj}$ are the mass matrix and the vector of the generalized force of the suspended object. $\boldsymbol{h}_{obj}\, \boldsymbol{k}_{obj}$ is the internal force caused by the kinematic redundancy of the UCDPR, and $\boldsymbol{h}_{obj}$ satisfies $\boldsymbol{G}_{obj}\, \boldsymbol{h}_{obj} = \boldsymbol{0}$. The term $\boldsymbol{k}_{obj}$ is an arbitrary vector expressing kinematic redundancy, which can be used to subtask the mechanism if appropriately determined by solving optimization problems related to the tension distribution of the UCDPR, trolley placement, and other features.[11]

### 4.2 Control system

The trajectory tracking control system of the UCDPR is configured as shown in Fig. 4. In Fig. 4, $\boldsymbol{q}_{obj}^{ref}$, $\dot{\boldsymbol{q}}_{obj}^{ref}$ and $\ddot{\boldsymbol{q}}_{obj}^{ref}$ are the reference trajectories of the suspended object. These reference trajectories are defined in Sect. 4.2.1 together with the UCDPR control objectives. About the virtual input $\boldsymbol{u}$, the positioning controller for Scenario A and the trajectory tracking controller for Scenario C are defined in Sect. 4.2.2. The optimization problem of calculating the kinematic redundancy parameter $\boldsymbol{k}_{obj}$ in Eq. (6) is formulated in Sect. 4.2.3.

#### 4.2.1 Control objective

First, we describe the design of the reference trajectory of the suspended object. As shown in a related study,[14] considering the actual control of trolleys and winches, if the manipulated variable $\boldsymbol{\kappa}$ and its first-order derivative (i.e., velocity) $\dot{\boldsymbol{\kappa}}$ are not continuous functions, the suspended object will vibrate. As shown in Eq. (5), $\boldsymbol{\kappa}$ includes the inverse kinematic solution $\boldsymbol{\lambda}_{obj}$ of Eq. (6). Therefore, $\boldsymbol{q}_{obj}$ should be continuous until jerked, i.e., a third-order differentiable. In this study, the reference path and reference trajectory of the suspended object were designed independently, using the parameter $s(t)$ ($0 \le s \le 1$), which explicitly includes the time $t$ ($0 \le t \le T$). Denoting the coordinates of the starting position of the path as $\boldsymbol{q}_{obj}^{init}$ and the coordinates of the ending position as $\boldsymbol{q}_{obj}^{fin}$, the reference trajectory of the suspended object is obtained using $s(t)$ as follows:

$$\boldsymbol{q}_{obj}^{ref}\left(s(t)\right) = \left(1 - s(t)\right)\boldsymbol{q}_{obj}^{init} + s(t)\boldsymbol{q}_{obj}^{fin}. \tag{7}$$

The path of the suspended object shown by Eq. (7) is the line connecting $\boldsymbol{q}_{obj}^{init}$ and $\boldsymbol{q}_{obj}^{fin}$ and is clearly a third-order differentiable. At the same time, $s(t)$ should also be a third-order differentiable, so $s(t)$ is given here as a seventh-order polynomial. Eight boundary conditions are

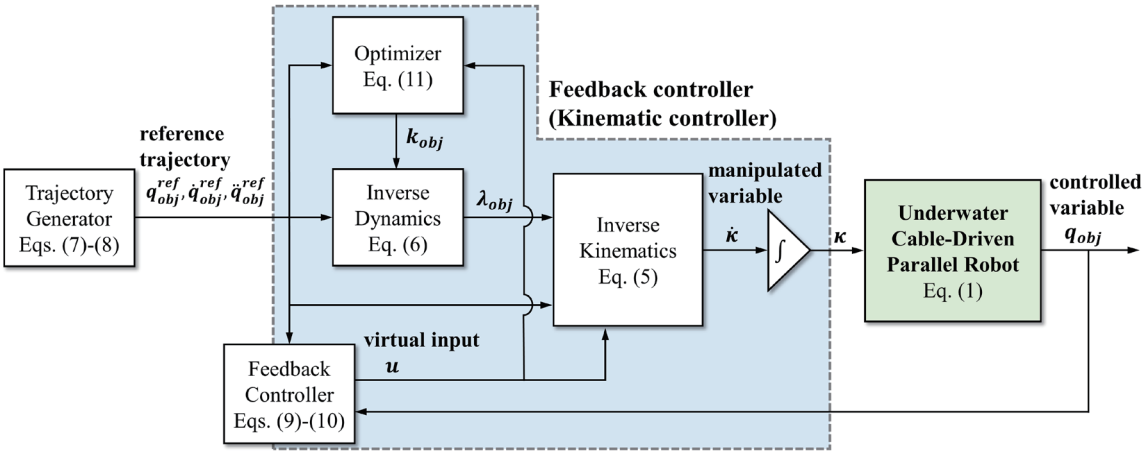


Fig. 4. (Color online) Block diagram of the trajectory tracking system.

needed to determine the coefficients of this polynomial. For these boundary conditions, $s(0) = 0$, so Eq. (7) becomes $\boldsymbol{q}_{obj}(0) = \boldsymbol{q}_{obj}^{init}$ at the start point of the path, and $s(T) = 1$, so that $\boldsymbol{q}_{obj}(T) = \boldsymbol{q}_{obj}^{fin}$ at the endpoint of the path. Also, $\dot{s}(0) = \dot{s}(T) = \ddot{s}(0) = \ddot{s}(T) = \dddot{s}(0) = \dddot{s}(T) = 0$, so that the suspended object stops at the start and end of the path (i.e., the velocity, acceleration, and jerk of the suspended object are all set to 0). On the basis of this analysis, the path parameter $s(t)$ is given by

$$s(t) = 35\left(\frac{t}{T}\right)^4 - 84\left(\frac{t}{T}\right)^5 + 70\left(\frac{t}{T}\right)^6 - 20\left(\frac{t}{T}\right)^7. \tag{8}$$

On the basis of this discussion, the reference trajectory of the suspended object is given in Fig. 5, where $\boldsymbol{q}_{obj}^{init} = [0.10,\ 0.30]^T$ and $\boldsymbol{q}_{obj}^{fin} = [0.40,\ 0.15]^T$. The 0 to 10 s phase is the positioning control phase of Scenario A, the 10 to 20 s phase is the trajectory tracking control phase of Scenario C, and the 20 to 30 s phase is for observing the residual vibration of the suspended object.

Next, we describe the control objectives of the numerical simulations. We designed the control system to stabilize the mechanism within 10 s after landing on water (Scenario A) and to track the reference trajectory of the suspended object shown in Fig. 5 within $\pm 10^{-2}$ m of position error (Scenario C) in the sea area with a maximum current velocity of 0.8 m/s ($\cong$ 1.5 knots).

### 4.2.2 Design of the controllers

The feedback controller in the following equation is the positioning controller used in Scenario A:

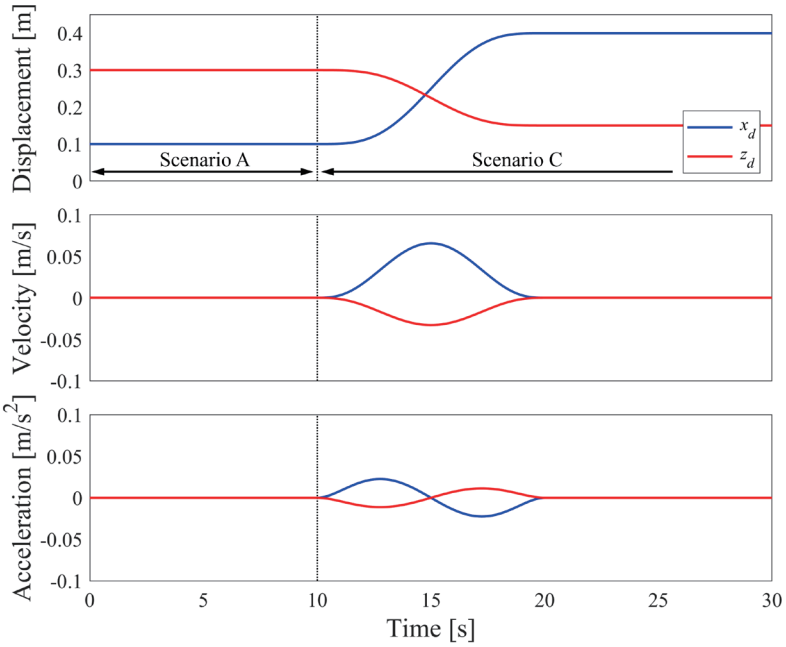


Fig. 5. (Color online) Reference trajectory of the suspended object.

$$\boldsymbol{u}_A = \boldsymbol{k}_A(\boldsymbol{q}_{obj}^{ref} - \boldsymbol{q}_{obj}). \tag{9}$$

Here, $\boldsymbol{k}_A$ is the feedback gain. The feed-forward + feedback controller in the following equation is the trajectory tracking controller used in Scenario C:

$$\boldsymbol{u}_C = \dot{\boldsymbol{q}}_{obj}^{ref} + \boldsymbol{k}_C(\boldsymbol{q}_{obj}^{ref} - \boldsymbol{q}). \tag{10}$$

Here, the first term on the right-hand side is the feedforward controller for trajectory tracking, and the second term is the feedback controller for reducing disturbances and modeling errors. The feedback gain $\boldsymbol{k}_C$ is given a high gain to reduce the effect of current and modeling errors caused by the dynamics of the cable. In general, this is called a high-gain feedback control [15] and is a simple method to improve the robustness of the control system. In this study, $\boldsymbol{k}_C$ is adjusted by trial and error for the motion of the UCDPR at the maximum current velocity of 0.8 m/s specified in the control objectives, and its effectiveness is verified in Sect. 4.3.

### 4.2.3 Optimization problem for redundancy parameter

The optimizer is designed to give the redundancy parameter $\boldsymbol{k}_{obj}$, which indicates the kinematic redundancy. We considered the optimization problem of the tension distribution of cables, which is often considered a subtask of the typical MCDPR.[3,11] The optimization problem of tension distribution in UCDPR is defined as

$$\begin{aligned}
&\min_{\boldsymbol{k}_{obj}} V = \boldsymbol{\lambda}_{obj}^T \boldsymbol{\lambda}_{obj} \\
&s.t.\ \ \boldsymbol{\lambda}_{obj} = \boldsymbol{G}_{obj}^{+T}(\boldsymbol{M}_{obj}\ddot{\boldsymbol{q}}_{obj} - \boldsymbol{F}_{obj}) + \boldsymbol{h}_{obj}\boldsymbol{k}_{obj} \\
&\qquad \dot{\boldsymbol{\kappa}} = \boldsymbol{J}_{obj}(\boldsymbol{q}_{obj}, \boldsymbol{\lambda}_{obj})\boldsymbol{u} \\
&\qquad \boldsymbol{\kappa} = \int \dot{\boldsymbol{\kappa}}\, dt \\
&\qquad 0 \le x_{vi} \le 0.7 \ (i = 1, 2) \\
&\qquad 0.10 \le x_{v2} - x_{v1}.
\end{aligned} \tag{11}$$

In this nonlinear optimization problem, $x_{vi}$ is the displacement of the trolley, and the inequality constraints are the range of motion of the two trolleys and the requirement that the two trolleys do not collide.

## 4.3 Simulation

Numerical simulations were performed using the control system described in Sect. 4.2. In this numerical simulation, the simulation environment was constructed using MATLAB/Simulink.

### 4.3.1 Variation of trajectory trackability in the case of uniform flow

Figure 6 shows the simulation results when the UCDPR tracked the reference trajectory shown in Fig. 5 underwater at a current velocity of 0.8 m/s. Figures 6(a)–6(c) show the results of the positioning control of Scenario A, and Figs. 6(d)–6(f) show the results of the trajectory tracking control of Scenario C. As shown in Fig. 6(a), the cable lengths and the position of the trolleys, which are determined from the geometric relationship of the UCDPR in static water, are given as appropriate initial values for the manipulated variables $\boldsymbol{\kappa}$ in the numerical simulation. In Figs. 6(a) and 6(b), the UCDPR swung from the initial position of the path due to the current, but by executing Scenario A, the state of the mechanism was stabilized as shown in Fig. 6(c) while

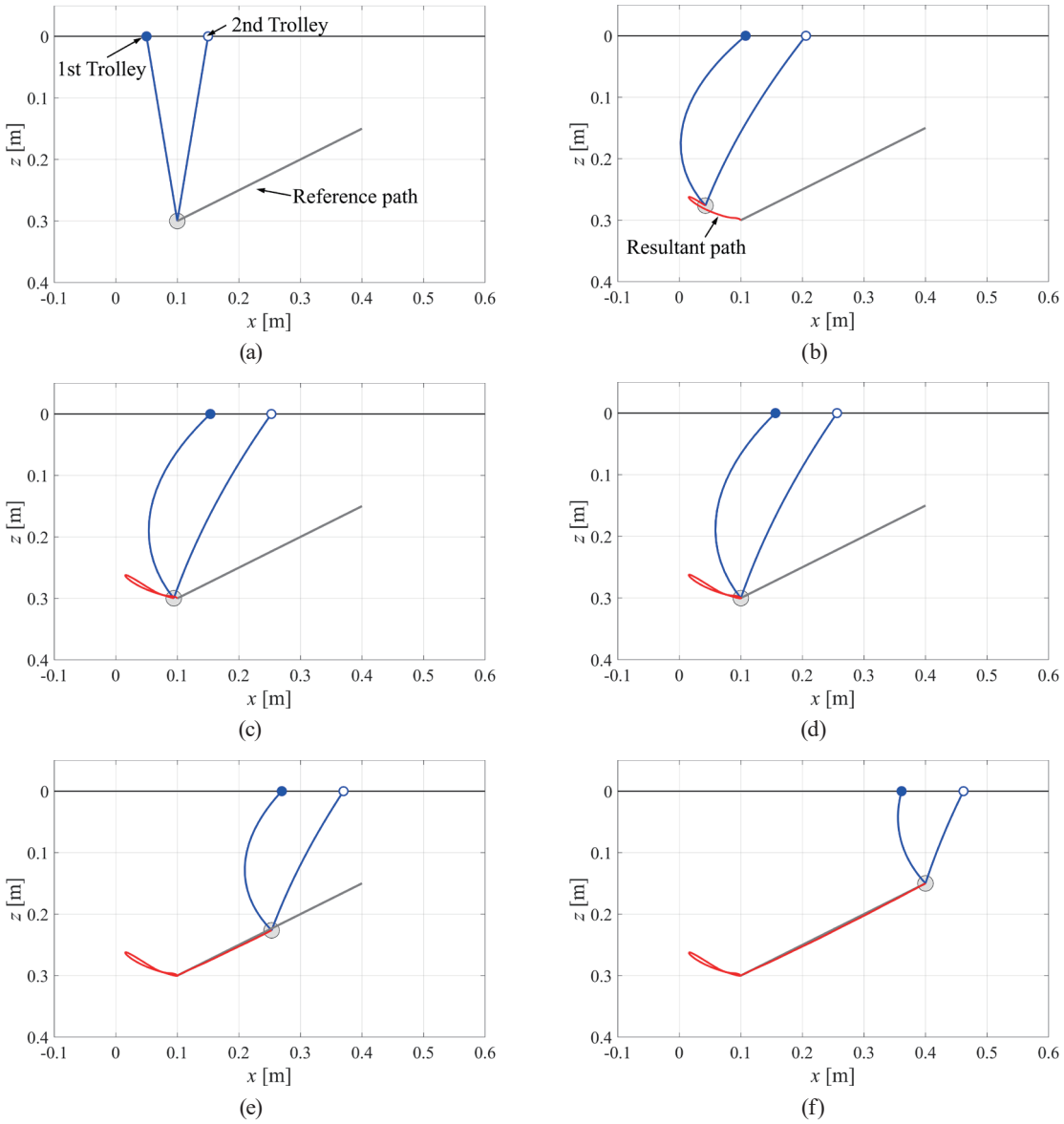


Fig. 6. (Color online) Simulation results for scenario A and scenario C (current velocity: −0.8 m/s). (a) $t$ = 0 s, (b) $t$ = 1.0 s, (c) $t$ = 3.0 s, (d) $t$ = 10.0 s, (e) $t$ = 15.0 s, and (f) $t$ = 20.0 s.

the effect of the current was reduced. In Figs. 6(d)–6(f), the UCDPR shifts to Scenario C and accurately tracks the preplanned reference path.

Figure 7 shows the variations of the tracking error for the numerical simulations for several current velocities. In Scenario A, the effect of the current velocity on the UCDPR was able to be reduced within a predefined time for velocities up to 0.8 m/s. After shifting to Scenario C, the position of the suspended object was able to be accurately tracked to the reference trajectory within the tolerance range. The maximum tracking error was observed around 15 s for all current velocities when the velocity of the reference trajectory was at its maximum.

Although the maximum current velocity was set at 0.8 m/s in the control objective in Sect. 4.1, the effect of the current velocity was reduced in a given time even when a disturbance of 1.2 m/s, which is outside the design range, was applied, and the tracking error was also kept within the tolerance range.

The numerical simulations in this study did not include considerations of constraints such as the maximum reeling speed of the winches and the speed of the trolley. In the future, it will be necessary to develop controllers that consider these constraints of the mechanism.

### 4.3.2 Variation of trajectory trackability with variation of flow velocity

Figure 8 shows the variation in the behavior of a suspended object and the tracking error when the current velocity was changed stepwise from 0.7 to 0.8 m/s ($t$ = 13 s). As shown in Fig. 8, the suspended object deviated strongly from the reference path due to the step change in current velocity during Scenario C and then converged at the end of the reference path with damped oscillations caused by the recovery motion. However, it takes a considerable amount of time for the suspended object to recover to the reference path.

These results indicate that a high-gain feedback controller improves the stability and the trajectory tracking performance of the control system but deteriorates other control features that have a trade-off relationship with the stability. In particular, the gain tuning has been done by trial and error for the motion of the UCDPR at a maximum current velocity of 0.8 m/s, which is defined as the control objective. Therefore, excessive robustness may have been given to the control system, resulting in a conservative system.

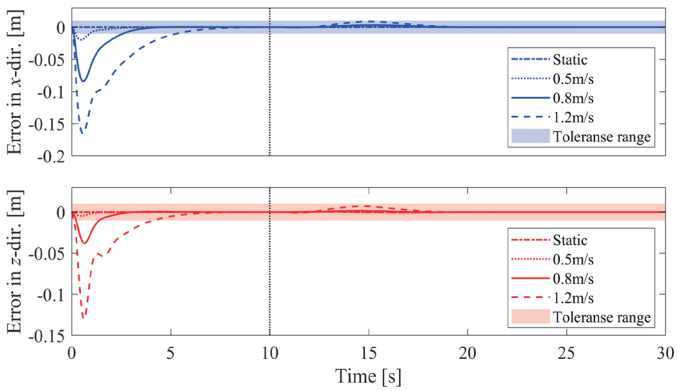


Fig. 7. (Color online) Comparisons of tracking errors.

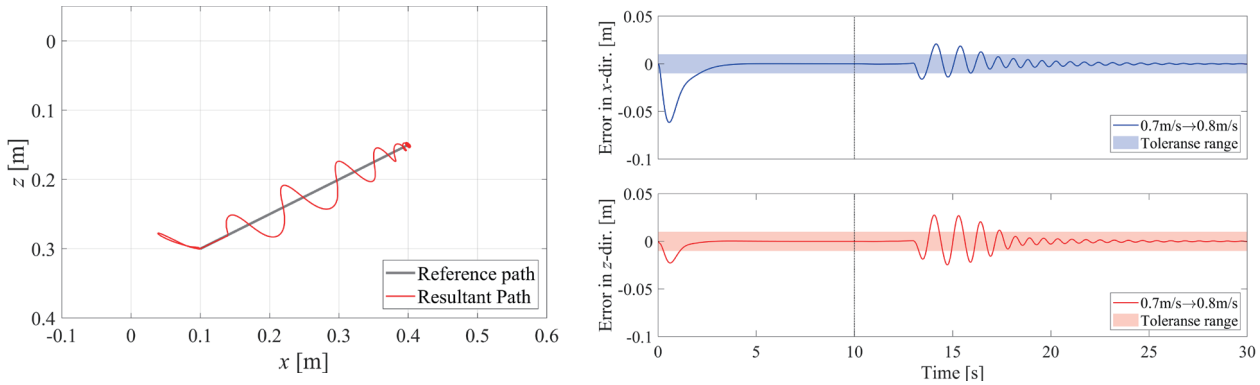


(a) (b)

Fig. 8. (Color online) Comparison of tracking error: (a) $t = 0$ s and (b) $t = 1.0$ s.

In general, the control parameter of high-gain feedback is reported to depend on unknown parameters such as the modeling error of the control model.[16] Excessive robustness was shown to cause degradation of control performance, so the high gain was developed into an adaptive control system that performs an online search based on control errors and other variables. In this way, it may be possible to achieve both optimal stability and control performance at all times while suppressing the effects of unknown parameters.

## 5. Conclusions

In this paper, we described an operational scenario for a UCDPR composed of multiple surface robots and assuming an actual environment. We simulated the control of the UCDPR in an operation scenario that included the control phase of positioning after landing on water (Scenario A) and the control phase of tracking along a predefined path (Scenario C).

Because the main purpose of this paper was to develop an operational scenario, a high-gain feedback controller was applied in the numerical simulation of Scenario C as a robust controller that is relatively easy to implement. As a result, it was found that while sufficient trajectory tracking was achieved for different current velocities in a uniform current, trajectory tracking deteriorated when the current velocity changed during the trajectory tracking.

The control system design and simulation in this study focused mainly on the current velocity as the only factor that changes the control performance of the UCDPR. However, in actual environments, other factors may have a strong effect on the performance, such as the effect of waves on surface robots, the stiffness of cables, and parameter errors of suspended objects.

The trajectory tracking controller in Eq. (10) is based on the kinematics around the suspended object. Therefore, even if the trajectory tracking of the suspended object is sufficient for a given reference path, there is no guarantee that it will be sufficient for a different reference trajectory because the inertia and other dynamic characteristics of the suspended object will change. In the future, we will develop an online retuning method of feedback gain based on adaptive control to solve these problems as well as that of the conservativeness of robust control and to verify a more active robust control method.

In addition, we discussed only control methods for Scenarios A and C. In the future, we will develop theories for online trajectory generation and guidance control methods for Scenario B and for determining the workspace for Scenario D.

## References


1 H. Kino and S. Kawamura: J. Robot. Mechatron. **27** (2015) 599. https://doi.org/10.20965/jrm.2015.p0599
2 H. Tachiya: Parallel Mechnism (Morikita-Syuppan, Tokyo, 2019) 1st ed., Chap. 8 (in Japanese).
3 Collaborative Mobile Cable-Driven Parallel Robots–Archive ouverte HAL: https://theses.hal.science/tel-02938097 (accessed January 2023).
4 N. Pedemonte, T. Rasheed, D. Marquez-Gamez, P. Long, E. Hocquard, F. Babin, C. Fouche, G. Caverot, A. Girin, and S. Caro: Advances in Robotics Research: From Lab to Market (Springer, 2020). https://doi.org/10.1007/978-3-030-22327-4_8
5 T. Rasheed, P. Long, D. Marquez-Gamez, and S. Caro: Proc. 4th Int. Conf. Cable-Driven Parallel Robots (Springer, 2019) 257. https://doi.org/10.1007/978-3-030-20751-9_22
6 N. Michael, J. Fink, and V. Kumar: Auton. Rob. **30** (2011) 73. https://doi.org/10.1007/s10514-010-9205-0
7 G. A. Cardona, D. Tellez-Castro, and E. Mojica-Nava: IFAC-PapersOnLine **52** (2019) 145. https://doi.org/10.1016/j.ifacol.2019.12.149
8 K. Kodama, A. Morinaga, and I. Yamamoto: Proc. SICE SI-2021 (SICE, 2021) 1488 (in Japanese).
9 K. Kodama, A. Morinaga, and I. Yamamoto: Proc. Robomech2022 (JSME, 2022) 2A1-B07 (in Japanese).
10 K. Kodama, A. Morinaga, and I. Yamamoto: J. Jpn. Soc. Nav. Archit. Ocean Eng. (JASNAOE) **36** (2022) 53 (in Japanese).
11 K. Kodama, A. Morinaga, and I. Yamamoto: Proc. SICE SI-2022 (2022) 929 (in Japanese).
12 M. Nakamura, T. Hyakudome, H. Yoshida, and T. Aoki: J. Jpn. Soc. Nav. Archit. Ocean Eng. **9** (2009) 139 (in Japanese). https://doi.org/10.2534/jjasnaoe.9.139
13 M. Nakamura, S. Ishibashi, T. Hyakudome, H. Yoshida, and T. Aoki: J. Jpn. Soc. Nav. Archit. Ocean Eng. **14** (2011) 143 (in Japanese). https://doi.org/10.2534/jjasnaoe.14.143
14 M. Yamamoto, N. Yanai, and A. Mohri: JRSJ **17** (1999) 1037 (in Japanese). https://doi.org/10.7210/jrsj.17.1037
15 H. Maeda: J. SICE **26** (1987) 381 (in Japanese). https://doi.org/10.11499/sicejl1962.26.381
16 S. Masuda: J. SICE **40** (2001) 717 (in Japanese). https://doi.org/10.11499/sicejl1962.40.717